Journal of Colloid and Interface Science 698 (2025) 138061

Contents lists available at ScienceDirect

Journal of Colloid And Interface Science

journal homepage: www.elsevier.com/locate/jcis

Regular Article

Protein nanorotors control the size of lipid domains in phase-separated monolayers

Nuria Carrillo-Godoy [a,b,c], David Valdivieso González [a,b,c], Paolo Natale [a,b,c], Hernán Ritacco [d], Francisco J. Cao-García [e,f], Víctor G. Almendro-Vedia [b,c,g], Iván López-Montero [a,b,c,*]

[a] Departamento de Química Física, Universidad Complutense de Madrid, 28040 Madrid, Spain
[b] Instituto de Investigación Biomédica Hospital 12 de Octubre (imas12), 28041 Madrid, Spain
[c] Instituto Pluridisciplinar, Universidad Complutense de Madrid, 28040 Madrid, Spain
[d] Instituto de Física del Sur (IFISUR), Departamento de Física, Universidad Nacional del Sur (UNS), CONICET, Av. L.N. Alem 1253, B8000CPB Bahía Blanca, Argentina
[e] Departamento de Estructura de la Materia, Física Térmica y Electrónica, Universidad Complutense de Madrid, 28040 Madrid, Spain
[f] IMDEA Nanociencia, 28049 Madrid, Spain
[g] Departamento de Farmacia Galénica y Tecnología Alimentaria, Universidad Complutense de Madrid, 28040 Madrid, Spain

HIGHLIGHTS

- ATP synthase protein nanorotor selectively localizes within cardiolipin-rich lipid phases.
- Rotation enlarges protein–rich domains and contracts protein-devoid domains.
- Size modulation follows the 2D Young-Laplace law via a protein-driven lateral pressure drop.
- Inhibiting rotation prevents size regulation, confirming activity-dependent control.
- Size modulation is triggered by surface pressure imbalances as low as 10^{-9} N/m.

GRAPHICAL ABSTRACT

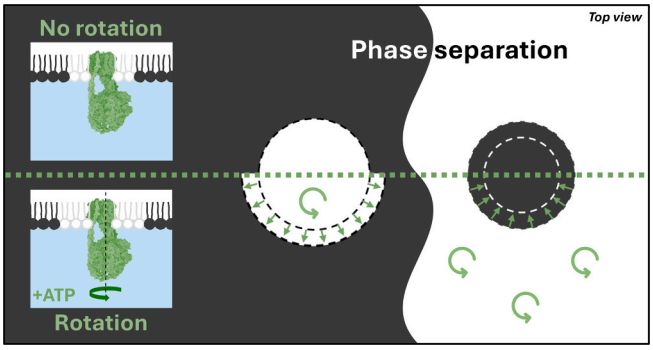

ARTICLE INFO

Keywords:
ATP synthase
Line tension
Lipid monolayers
Domains
Rotation
Biological spinners
Lateral pressure

ABSTRACT

Hypothesis: Phase separation in lipid membranes leads to the formation of distinct lipid domains, which are influenced by kinetic factors and interfacial phenomena. While line tension has been considered a key determinant of domain size, studies suggest that kinetic effects play a significant role. We hypothesize that modifying *in situ* the surface pressure difference between coexisting lipid phases can regulate domain size. Specifically, the rotational activity of ATP synthase embedded in a specific phase may induce local changes in the lipid surface pressure, triggering the change in domain size.

Experiments: To test this hypothesis, ATP synthase was incorporated into phase-separated lipid monolayers by leveraging its specific interaction with cardiolipin (CL). The ATP synthase assembly and its co-localization within CL-rich phases were characterized to assess the enzyme's role in domain modulation. The effect of rotational forces on phase dynamics was analyzed, with particular attention to the change in size of protein-enriched and

* Corresponding author at: Departamento de Química Física. Universidad Complutense de Madrid, 28040 Madrid, Spain.
E-mail address: ivanlopez@quim.ucm.es (I. López-Montero).

https://doi.org/10.1016/j.jcis.2025.138061
Received 19 March 2025; Received in revised form 31 May 2025; Accepted 1 June 2025
Available online 2 June 2025

protein-devoid lipid domains. The system was characterized using fluorescence video microscopy and quantitative analysis of domain contour fluctuations.
Findings: Upon ATP addition, protein-enriched domains increased in size, while protein-devoid domains contracted. The observed changes followed the 2D Young-Laplace equation, where the spinning motion of ATP synthase reduces the lateral pressure in the protein-enriched phase. The unbalanced surface pressure between phases drives the domain size modulation; which is sensitive to variations in the surface pressure difference between lipid phases as small as 10^{-9}N/m. These findings show that ATP synthase activity can dynamically regulate lipid phase separation by modifying interfacial properties and kinetic constraints.

1. Introduction

Phase separation in lipid membranes occurs when different lipid species segregate into distinct domains [1]. The formation of lipid domains occurs in two particular steps. Initially, during the nucleation phase, fluctuations within a uniform lipid medium lead to the emergence of small nuclei of a new phase. If these nuclei exceed a critical size, they continue expanding by absorbing material from the surrounding membrane. As this process develops, the concentration of the continuous phase decreases, eventually preventing the formation of additional nuclei. The kinetics of phase separation is extremely rapid, occurring within 10^{-4} s and 10^{-3} s for nucleation and growth stages, respectively [2]. Interestingly, both timescales are independent of the area fraction of the forming phase. Consequently, the resulting domain size distribution can be heterogeneous. In other words, the number and size of domains are influenced by how abruptly the system reaches a specific point in the surface pressure–temperature ($\pi - T$) phase diagram. Faster transitions lead to the development of more nuclei. For instance, increasing the compression rate of a lipid monolayer has been shown to increase the number of domains formed [3]. Likewise, the rate at which the critical temperature is reached plays a crucial role in domain formation [4].

After stabilization, mass redistribution within the system may occur over extended timescales (ranging from minutes to hours) through two primary mechanisms: Ostwald ripening and coarsening. Both processes are governed by the 2D Young-Laplace equation, $\Delta\pi = \frac{\gamma}{R_0}$, where $\Delta\pi$ represents the surface pressure difference across the two phases (higher inside; i.e. $\Delta\pi = \pi_i - \pi_o$), γ is the line tension of the interface and R_0 is the radius of the lipid domain. In systems with a broad distribution of domain sizes, excess line energy drives the minimization of total interfacial energy, favoring complete phase separation and reducing the contact border between phases to its minimum extent. Ripening occurs as smaller, high-energy domains dissolve and transfer their material to larger, more stable domains, promoting their growth. In contrast, coarsening involves the merging of neighboring domains. The coalescence of domains depends on their mobility and the strength of their long-range repulsive interactions, both of which vary across different membrane models. As a result, domains can merge into one large domain within seconds in unilamellar vesicles [5], whereas in monolayers, merging of domains may take hours. Thus, domain distribution remains stable in monolayers for extended periods due to differences in dipole density between lipid phases [6,7]. This slow evolution of lipid domains makes it difficult to distinguish kinetically trapped states from equilibrium phases.

Since line tension determines the energy cost of increasing interfacial contact, it should play a key role in defining domain size. Similar to its 3D analogue, line tension depends on phase composition and mixing ability. In lipid membranes, hydrophobic mismatch between coexisting phases correlates with domain size in model bilayers [8,9]. Specifically, higher hydrophobic mismatch might lead to higher line tension and smaller domains. Also, the addition of the so-termed “lineactants” or hybrid lipids to the lipid mixture regulates domain size by diminishing the interfacial tension and hence reducing the packing incompatibility [10,11]. However, some studies show that reducing line tension by an order of magnitude through “lineactant” incorporation does not significantly alter size distribution [9,12], suggesting that domain size is influenced by kinetic factors as well. To better control lipid domain size, we hypothesize that altering surface pressure differences across phases could provide precise regulation. Specifically, we propose designing a driven system in which functional proteins are incorporated within a specific phase, allowing their activity to selectively influence only one phase of the lipid system.

Among protein-based machines, F_1F_o-ATP synthase (ATP synthase) is the most crucial biological motor with rotational movement [13]. Found in the inner mitochondrial membrane of eukaryotes and the plasma membrane of prokaryotes, ATP synthase synthesizes adenosine triphosphate (ATP) — the cell’s primary energy molecule — through oxidative phosphorylation [14]. This process involves the rotation of the membrane embedded F_o domain, driven by a proton gradient that is produced by the electron transport chain. The enzyme converts adenosine diphosphate (ADP) and inorganic phosphate (P_i) into ATP. Remarkably, the motor is reversible, prompting the reverse rotation with excess of ATP [15].

The rotation of ATP synthase’s F_o domain not only powers ATP production but also influences the surrounding lipid bilayer, affecting its structural and elastic properties. Similar to macroscopic spinners [16,17,18], membranes with protein nanorotors exhibit emergent effects [19,20]. Importantly, the spinning movement ATP synthase can induce local deformations and changes in membrane surface pressure [21], which affect the overall elasticity of the lipid membrane, producing non-equilibrium membrane fluctuations [22] or the curvature sorting of rotating proteins [23]. This ability makes ATP synthase a suitable candidate to test the impact of rotating forces in phase-separated membranes.

The paradigmatic lipid composition for phase separation in lipid monolayers typically involves a mixture of a high-melting-temperature saturated lipid such as dipalmitoylphosphatidylcholine (DPPC), a low-melting-temperature unsaturated lipid such as dioleoylphosphatidylcholine (DOPC), and cholesterol, forming liquid-ordered (L_o) and liquid-expanded (LE) phases [24]. Building on the classic lipid mixture used to study phase separation, a new composition incorporating heart bovine cardiolipin (CL) offers additional insights into membrane-protein interactions. CL, a negatively charged phospholipid with four fatty acid chains, binds specifically to ATP synthase [25,26]; which might facilitate the targeted incorporation of the enzyme into CL-rich phases. This specific interaction enables a controlled experimental framework in which ATP synthase can be strategically localized within defined lipid phases.

The objective of this study was to examine how the rotational activity of ATP synthase influences the lateral organization of phase-separated lipid monolayers. By reconstituting purified *E. coli* ATP synthase [27] into cardiolipin-enriched liposomes and forming monolayers at the air–liquid interface, we assessed whether protein activity affects domain size and distribution. To confirm the role of rotary motion, we compared conditions with and without ATP, as well as with a specific inhibitor blocking ATP synthase activity, allowing us to distinguish active, rotation-driven effects from passive lipid–protein interactions. Building on our observations, the changes in size of lipid domains by the rotary motion of ATP synthase follows the 2D version of the Young Laplace equation. Specifically, the spinning movement of ATP synthase drops the lateral pressure of the protein-enriched phase [21], which

drives the size modulation of domains as an attempt to compensate the unbalanced surface pressure difference across the fluid–fluid interface.

2. Materials and methods

2.1. Chemicals

Potassium chloride (KCl), magnesium chloride ($MgCl_2$), 4-(2-hydroxyethyl) − 1-piperazineethanesulfonic acid (HEPES), N,N′-dicyclohexylcarbodiimide (DCCD), Adenosine 5′-triphosphate disodium salt (ATP) were supplied by Sigma-Aldrich. Alexa 488-NHS was acquired from Thermo Fisher (Molecular Probes). Ultrapure water was produced from Milli-Q unit (Millipore, conductivity lower than 18 MΩ cm^{-1}).

2.2. Lipids

1,2-dioleoyl-*sn-glycero*-3-phosphoethanolamine-N-(lissamine rhodamine B sulfonyl) (ammonium salt) (RhPE), 1,2-dipalmitoyl-*sn-glycero*-3-phosphocholine (DPPC), 1,2-dioleoyl-*sn-glycero*-3-phosphocholine (DOPC), cholesterol and 1′,3′-bis[1-*palmitoyl*-2-*oleoyl-sn-glycero*-3-*phospho*]-glycerol (Heart bovine, sodium salt) (CL) were purchased from Avanti Polar. Lipids were suspended in chloroform at 1 mg mL^{-1} and stored at − 20 °C.

2.3. Protein purification and fluorescent labelling

Bacterial F_1F_o–ATP synthase was purified from native *E. coli* MG1655 cytoplasmic membranes as described in [27] and fluorescently labelled with fluorescent Alexa 488-NHS as described in [22]. Labelled proteins were conserved in stock solution (200 mM sucrose, 10 mM KCl, 10 mM Tris HCl pH 8, 0.5 mM DDM) at − 80 °C.

2.4. SUVs preparation

Small unilamellar vesicles (SUVs) were prepared using the film lipid film hydration method followed by ultrasonication. Desired solution of lipids suspended in chloroform (DPPC/Chol/DOPC (50/30/20) or DPPC/Chol/DOPC/CL (50/30/10/10); % mol) was deposited in a flask after which the organic solvents were evaporated off under vacuum at 60 °C for 10 min. The hydration of lipids was performed by adding 250 μL of Milli-Q water to the flask containing the dry lipid film allowing hydration to occur at room temperature. Solution was sonicated in an ice-water bath, to avoid heating of the sample with an ultrasonic tip sonicator for 10 min set to 30 % power cycle with a pulse length time 5 min alternating 5 s on and 5 s off cycles.

2.5. Reconstitution of ATP synthase in proteoliposomes

Protein reconstitution into SUVs was performed by incubation of the protein with vesicles at a protein-to-lipid molar ratio of 1:10,000 for 45 min at 4 °C under continuous agitation. The protein lipid mixture was centrifuged at 80,000 rpm for 30 min and pellet was resuspended in HEPES 20 mM pH 7.4. Solution was put through four cycles of 5 s of sonication followed by 5 s of cooling in ice.

2.6. Compression isotherms

Lipid monolayers were formed onto the air–water interface by dropwise deposition from a Hamilton syringe of lipids suspended in chloroform at 0.17 mM. Water subphase contained 150 mM KCl, 500 mM $MgCl_2$ and 20 mM HEPES pH 7.4. Lipid mixtures of DPPC/Chol/DOPC (50/30/20), DPPC/Chol/DOPC/CL (50/30/15/5) or DPPC/Chol/DOPC/CL (50/30/10/10) (% mol) were deposited in a teflon bath of a Langmuir-Blodgett Nima 611 Trough. The monolayer was allowed to rest with the barriers fully expanded for 10 min for solvent evaporation. Surface pressure and area were recorded during isothermal compression at a barrier speed of 10 cm^2/min.

2.7. Monolayer formation by spreading lipids or proteoliposomes

Several μL of suspended solution of lipids in chloroform or proteoliposomes were spread dropwise on the air–water interface to achieve a surface pressure of 20 or 30 mN/m. Lipid compositions were DPPC/Chol/DOPC (50/30/20) or DPPC/Chol/DOPC/CL (50/30/10/10) (% mol). For active conditions, ATP was added (3.45 mM ATP final concentration) into the water subphase after film recording of passive ATP synthase lipid monolayers. For F_o inhibition experiment, the same external media used for active conditions was complemented with DCCD (1 mM final concentration).

2.8. X-ray reflectometry

Again, prior to any measurements, lipid monolayers were spread dropwise from solution of lipids in chloroform or proteoliposomes onto the air–water interface to the desired surface pressure. Lipid compositions were DPPC or DPPC/Chol/DOPC/CL (50/30/10/10) (% mol). X-ray reflectometry (XRR) measurements were performed using an Empyrean III apparatus (Malvern-Panalytical) adapted for XRR measurements in liquids, following the setup described in [28]. Preliminary experiments were conducted in the setup available at UNS (Argentina) and later completed at Unidad de Rayos X (UCM, Spain), using the same equipment and setup developed at UNS. The instrument operates at a wavelength of 1.54 Å, generated by a sealed X-ray tube. A focusing X-ray mirror with line collimation (1/32″ Mo slit) was employed to enhance beam intensity. The device is equipped with a PIXcel 3D detector used in 0D mode with only five active channels, attached to a parallel plate collimator (PPC). A 10 mm mask was used in all experiments. The omega-2theta (Ω-2θ) angle was varied between 0.1° and 8° with a step size of 0.0016° and a measurement time of 1.5 s per step, covering a scattering vector range of approximately $0.004 < q < 0.57$ $Å^{-1}$. A specific protocol was followed to align the incident X-ray beam with the liquid interface periodically to minimize evaporation effects, as described in [28]. All experiments were conducted at room temperature (~ 25 °C).

All data were first fitted and analyzed using a stochastic model-independent (MI) method, followed by model-dependent (MD) fitting, which was implemented based on the MI results to directly fit the electron density profiles obtained from MI calculations [36]. For this, we used the StochFit software (REF: https://stochfit.sourceforge.net/). StochFit segments the electron density profile into numerous small boxes and stochastically varies their electron densities to determine the best fit to the measured reflectivity. Additionally, it enables model-dependent fitting by performing a stochastic search of the parameter space to identify the optimal fit. In StochFit, both MI and MD fitting routines rely on reflectivity calculations using a recursive method first proposed by Parratt [29]. As mentioned, the electron density profile is divided into very thin layers (<1 Å), and the reflectivity at each layer is determined by considering the contributions of the layers beneath it, starting from the subphase and progressing to the superphase. As a result, the final reflectivity at the interface is derived from the cumulative effect of all underlying layers on the electron density profile so calculated. Once the MI fitting meets the required quality criteria, a model-fitting approach is selected to fit the resulting electron density profile. In this work, all XRR data were fitted using a two-layer model.

2.9. Fluorescence microscopy

Confocal microscopy images were collected with a Nikon Ti-E inverted microscope equipped with a Nikon C2 confocal scanning confocal module, 488-nm and 561-nm continuous lasers, emission band-pass filters (525 / 50 and dichroic 561LP for the green and red channel, respectively) and a Nikon LWD Lambda S 40XC water immersion

objective. Domains were imaged using the Nikon Ti-E inverted microscope in wide-field fluorescence mode equipped with a Niji LED light source (Blue Box Optics Ltd) and an ultrafast Zyla 4.2 sCMOS camera (Andor Technology) at 10–20 fps. Monolayers were prepared in a 1 mL pool with a 12.56 cm^2 area and a small thickness of the water subphase consistent with the objective working distance (0.61–0.59 mm).

2.10. Contour analysis and line tension determination

The line tension, γ, of quasi-circular domains can be determined from the thermal fluctuations of their average radius (R_0). A series of movies of protein rich and protein-devoid domains were analyzed with a MATLAB script to detect and parameterize the boundary fluctuations using a harmonic series in polar coordinates $R(\phi) = R_0$; where $a_{n,t}$ and $b_{n,t}$ are the Fourier coefficients for each mode n of a particular frame at time t. R_0 is defined as the radius of a circle $A = \pi R_0^2$ with an equivalent surface area of the domain. The optimal number of modes to describe the contour of domains was $n = 12$. Additional number of modes did not result into a significant change on the line tension value. The line tension of each protein domain was obtained by fitting the experimental time-averaged amplitudes to the theoretical spectrum derived from the equipartition theorem to capillary waves [38]:

$$\langle a_n^2 \rangle + \langle b_n^2 \rangle = \frac{2k_B T}{\pi R_0 \gamma}\left(\frac{1}{n^2 - 1}\right)$$

3. Results and discussion

3.1. Characterization of phase-separated lipid monolayers made of CL-enriched lipid compositions

To determine the phase behaviour of spread proteoliposomes we first explored whether CL could impair the canonical lipid composition to phase separate as long as CL replaced DOPC. We first built the surface pressure-area (π-A) isotherm of Langmuir monolayers composed of the ternary lipid mixture DPPC/Chol/DOPC (50/30/20 % mol) (Fig. 1A). Although the resulting isotherm did not exhibit a horizontal plateau characteristic for phase coexistence, fluorescence microscopy revealed the presence of lipid domains above surface pressure $\pi > 15 mN/m$; in agreement with the ternary phase diagram in lipid monolayers at the air–liquid interface [24]. Rhodamine-PE was used to reveal LE domains as this dye partitions into the expanded phase and excluded from the cholesterol-rich L_o phase. Close to the surface pressure of $\pi = 20 \pm 2 mN/m$, the monolayer exhibited similar fractions of bright (low cholesterol) or dark circular (high cholesterol) domains on a dark or bright background, respectively.

To mimic the amount of CL found in native membranes (around 10 % mol) [30,31] two different π-A isotherms were obtained by replacing DOPC with CL and keeping constant the molar ratio of Chol and DPPC (Fig. 1A). As the four unsaturated acyl chains of CL require more area than the two unsaturated chains of DOPC, monolayers containing CL presented bigger molecular areas. Again, the resulting isotherms exhibit a liquid-expanded state but the presence of phase coexistence over a broad range of surface pressures was also imaged by fluorescence microscopy. At the packing state of $\pi = 20 \pm 2 mN/m$; the distribution of dense domains in a fluid continuous phase or vice versa was not affected by the presence of CL as visualized by fluorescence microscopy. Additionally, the compressibility modulus for each lipid composition were obtained as the numerical derivative of isotherms; $C_S^{-1} = A\left(\frac{\partial \pi}{\partial A}\right)_T$ (Fig. 1B). Whereas the addition of CL preserves a similar compressibility at low lateral pressures ($\pi \leq 20 mN/m$) it endows the monolayer with a lower compressibility modulus at higher packing states ($\pi > 20 mN/m$). CL modulates the mechanical properties of phospholipid membranes [32,33,34,35]. Its characteristic diphosphatidylglycerol structure with four acyl chains contributes to the expansion of compression isotherms in various PC/CL and PE/CL lipid monolayers

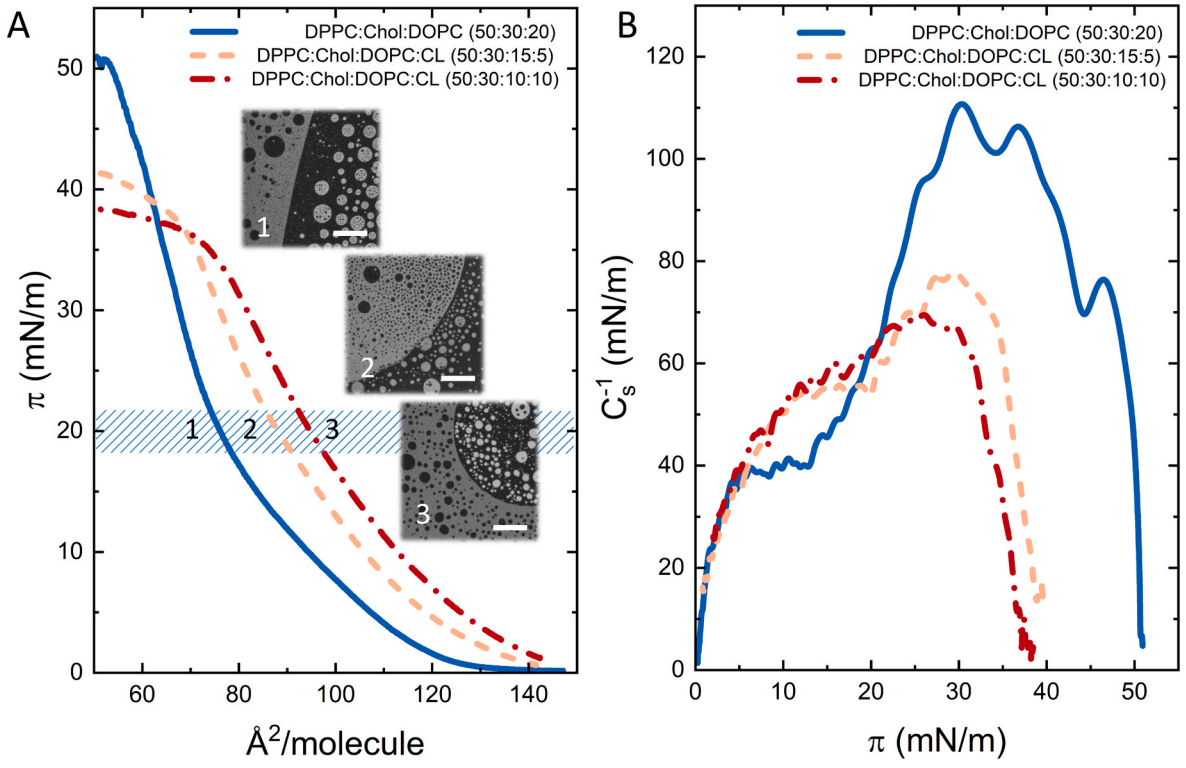

Fig. 1. A) π − A isotherms of DPPC/Chol/DOPC (50/30/20 % mol), DPPC/Chol/DOPC/CL (50/30/15/5 % mol) and DPPC/Chol/DOPC/CL (50/30/10/10 % mol) lipid monolayers at 22 °C and at compression rate of 10 cm^2/min. **B)** Compressibility modulus, C_S^{-1} as a function of the surface pressure of the same monolayers shown in A).

[32,33,35]. As a result, while CL may lower the collapse pressure, it enhances mechanical elasticity, which corresponds to a more expanded lateral organization [33,35]. Hereinafter, the lateral pressure of $\pi = 20 \pm 2mN/m$ was chosen as a reliable descriptor of both the lipid packing and mechanical state, as all monolayers exhibit similar structural and mechanical properties at this pressure. In particular, phase separating monolayers containing 10 % mol of CL were used for protein incorporation.

3.2. ATP synthase localizes and incorporates in CL-enriched phases of lipid monolayers at the air –liquid interface

One approach to forming lipid-protein monolayers might result from injecting the protein into the subphase beneath the air–liquid interface and allowing it to adsorb onto the lipid layer. However, this method introduces several challenges, including a limited control over the lipid-to-protein ratio and the potential for proteins to modify unpredictably the phase behaviour of the preformed lipid monolayer. Additionally, the process requires detergents to facilitate protein solubility and adsorption, which can alter the interfacial properties of the lipid monolayer and compromise the integrity of the experimental setup. By instead spreading proteoliposomes directly onto the interface, we eliminate the need for detergents and retain precise control over lipid-protein composition, enabling a more stable and accurate model for studying interfacial properties. Here, proteoliposomes were made of DPPC/Chol/DOPC/CL (50/30/10/10 % mol) with a lipid-to-protein ratio of L/P = 10,000 (see Methods). To form the monolayer, several microliters of proteoliposomes were then carefully spread drop-wise to the air–liquid interface at a final surface pressure of $\pi = 20mN/m$. (Fig. 2A).

To confirm the presence of proteins and their preferred location within the phase-separated lipid monolayers formed from proteoliposomes, ATP synthase was fluorescently labelled with Alexa-488 (green channel) and lipids were doped with RhPE (red channel). After spreading and equilibration at a surface pressure of $\pi = 20 \pm 2mN/m$, the lipid monolayer exhibited distinct phases with the protein preferentially localizing within the CL-enriched phase (red channel) (Fig. 2B). Colocalization analysis of the fluorescence channels revealed that the green fluorescence from the protein overlapped significantly with the red fluorescence from the CL-rich regions, indicating selective incorporation of the protein into this specific lipid phase. This colocalization underscores the affinity of the protein for the CL-enriched areas within the phase-separated monolayer [25,26]. To assess the specificity of this interaction, a control experiment was performed using lipid monolayers lacking CL. In the absence of CL, the distribution of ATP synthase changed notably. The green fluorescence signal was detected in both the L_o and LE phases, indicating a broader and less selective partitioning of the protein. This contrasts with the CL-containing monolayers, where the protein showed a clear preference for the CL-enriched LE phase (Fig. S1). These findings suggest that the presence of CL enhances the selective incorporation of ATP synthase into the expanded regions of the monolayer, highlighting a specific interaction that is absent when CL is removed.

To verify the monolayer structure at the air–liquid interface after spreading proteoliposomes, we conducted X-ray reflectometry (XRR) experiments (Fig. 3). Initial measurements on pure lipid monolayers containing 10 mol% CL were performed after spreading the lipid molecules onto the air–liquid interface, using chloroform as a volatile organic solvent. Although lipid monolayers can exhibit phase separation (Fig. 1), the reflectivity measurements provide averaged information over the area illuminated by the incident X-ray beam due to the drift motion of the monolayer. Consequently, the detected signal represents an average electron density profile of the components present within the illuminated region and can be analyzed using the optical matrix StochFit method and software [36] (see Methods).

In this model-independent fitting process, the monolayer's electron density is represented as a series of thin slabs with constant electron densities. These densities are adjusted to optimize a mathematical model that closely matched the normalized XRR intensities (Fig. 3A). The best

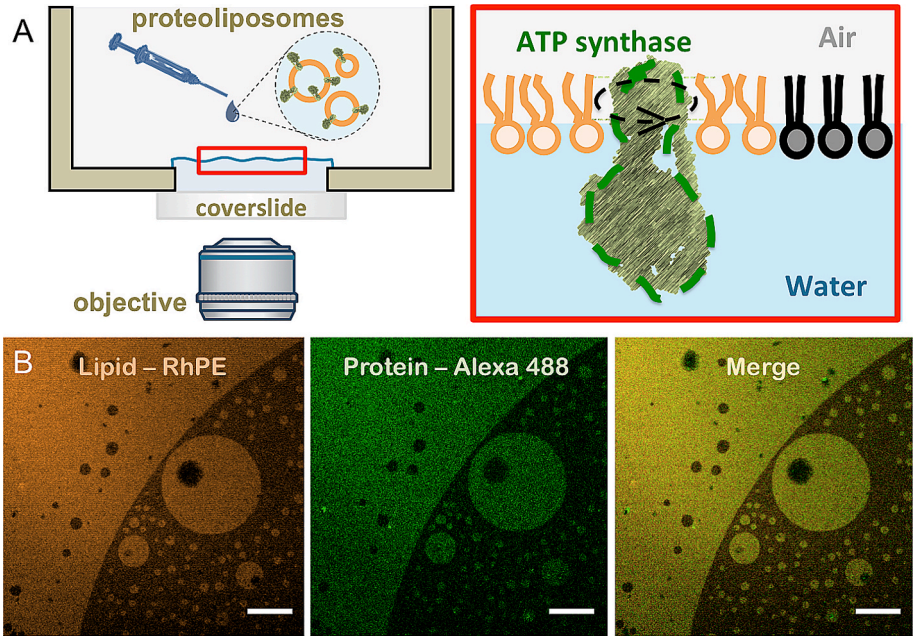

Fig. 2. A) Diagram the experimental setup of the air–water interface and fluorescence microscopy. Lipid mixtures dissolved in chloroform or proteoliposomes are spread at the air–water interface forming a monomolecular layer. In independent dropwise deposition experiments, the volume required to reach a particular surface pressure is obtained using a Wilhelmy plate. **B)** Fluorescence micrograph of a phase separated monolayer of DPPC/Chol/DOPC/CL (50/30/10/10 % mol) with a lipid-to-protein ratio of L/P = 10,000 at 20 mN/m. The LE phase (red channel) was labelled with the fluorescent lipid RhPE, whereas the protein was labelled with Alexa-488. Merge show a significant colocalization of ATP synthase in the LE phase, likely driven by the specific interaction with CL. The monolayer exhibits areas of similar fractions of bright (LE) and dark (L_o) domains. The scale bars are 10 μm. (For interpretation of the references to colour in this figure legend, the reader is referred to the web version of this article.)

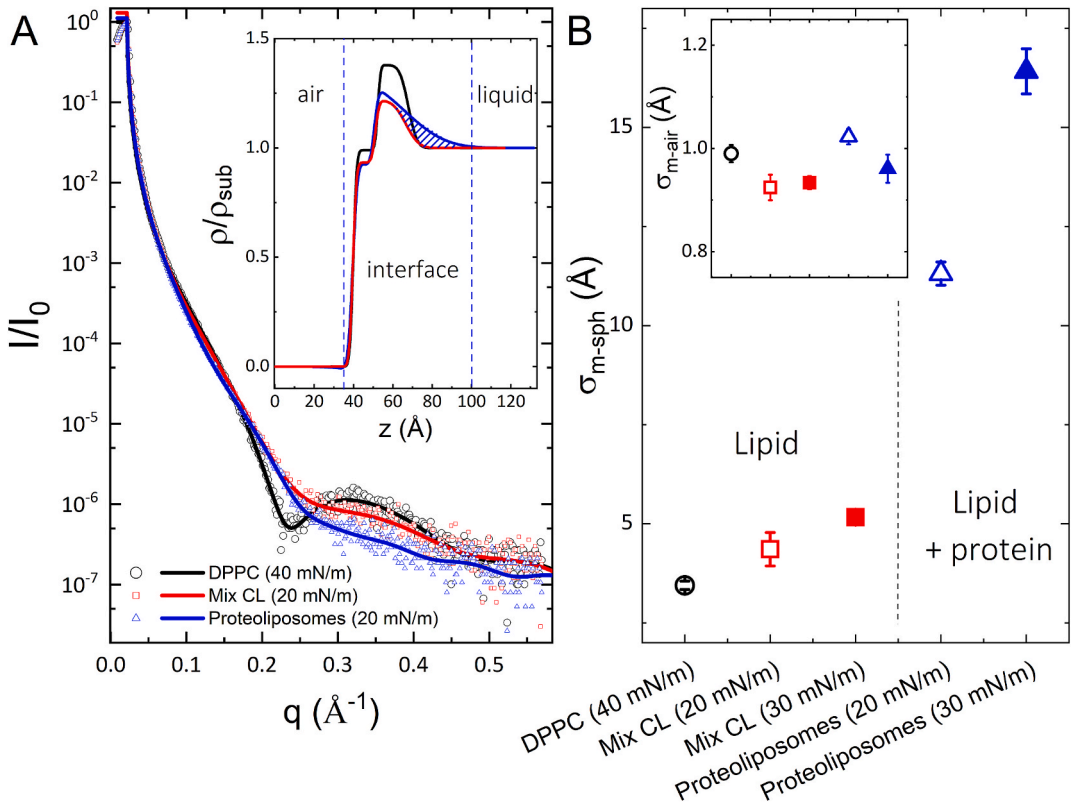

Fig. 3. A) Superimposed curves of normalized X-ray reflectivity for pure DPPC (40 mN/m, empty circles), DPPC/Chol/DOPC/CL (50/30/10/10 % mol, 20 mN/m, empty squares) lipid monolayers and the monolayer obtained by spreading proteoliposomes (20 mN/m, empty triangles). The points are the experimental results and the lines are the fitting curves using Stochfit software. **Inset**: Normalized electron density profiles as obtained from the XRR curves of the same monolayers in A), by fitting with a two-slab model. The electron densities $\rho(z)$ are normalized to the electron density of buffer subphase. Shaded region represents the increase in electron density by the presence of ATP synthase **B)** Roughness of the subphase-monolayer interface (σ_{m-sph}) for all the monolayers studied, showing the changes with lateral pressure and by the inclusion of the ATP-synthase protein. **Inset**: Roughness of the monolayer-air interface (σ_{m-air}) for the same samples in B).

fit minimizing the χ^2 value provided a smooth electron density profile aligned with the experimental data. For pure lipid monolayers, two slabs were sufficient to model the XRR profiles: the hydrophilic headgroup region and the hydrophobic tail region (Fig. 3A, inset). The model includes as fitting parameters the total thickness (d), the electronic density along the perpendicular direction ($\rho(z)$) and both the rugosity in the monolayer-liquid (σ_{m-sph}) and monolayer-air (σ_{m-air}) interfaces, respectively. For comparison, we also measured a DPPC monolayer at high surface pressure of $\pi = 40 \pm 2 mN/m$, ensuring that the lipid monolayer is in the liquid-condensed (LC) phase. In this phase, the XRR curve typically exhibits well-defined interference fringes (Kiessig oscillations) due to the high packing density and reduced roughness of the monolayer, indicating a uniform electronic density profile, which is indicative of a more uniform and ordered interface.

The resulting fits (Fig. 3A), yield a total thickness of $d_{DPPC} = 28 \pm 1$Å for the DPPC monolayer, with low monolayer-subphase interface roughness ($\sigma^{DPPC}_{m-sph} \approx 3$Å, Fig. 3B), consistent with values reported in the literature [37]. For the lipid mixture DPPC/Chol/DOPC/CL (50/30/10/10 % mol) at a lateral pressure of 20 mN/m, the thickness remains similar to that of DPPC monolayers ($d_{CLmix} = 27 \pm 1$Å). However, the monolayer-subphase interface roughness is slightly higher ($\sigma^{CLmix}_{m-sph} \approx 4$Å) (Fig. 3B), likely due to the presence of multiple lipid components with varying electronic densities and sizes. This compositional heterogeneity leads to a less uniform electronic density, which is captured as an increased roughness by the fitting model. Notably, σ_{m-air} remains largely unchanged (Fig. 3B, inset).

The incorporation of proteoliposomes altered the XRR profiles (Fig. 3A). As the reflected signal at low values (larger distances) remained unchanged, the formation of a bilayer or three-layered structure at the air–liquid interface can be excluded. A key observation was a more pronounced decay in the reflected intensity at higher q values compared to the pure lipid monolayer, suggesting increased height fluctuations at the molecular scale. As the monolayer thickness remained similar, $d_{Proteolip} = 26 \pm 1$Å, ATP synthase disrupts the ordered lipid monolayer, causing local variations in electron density due to heterogeneous protein insertion. The structural complexity of ATP synthase likely causes protrusions and depressions, increasing roughness and the observed decay is indicative of protein incorporation in the lipid monolayer.

The modelling of the electron density profiles provides quantitative insights into the structural impact of ATP synthase integration (Fig. 3A, inset). Due to the low protein ratio, we fitted the XRR data using the same two-slab model, accounting for the electron density and roughness at both the monolayer-liquid and monolayer-air interfaces. This approach ensures that the ensemble-averaged data effectively captures the interfacial changes compared to pure lipid monolayers. First, the increase in σ_{m-sph} from 4 Å to 11 Å confirms that ATP synthase integration introduces nanoscale roughness (Fig. 3B), altering the overall monolayer organization. The roughness values of the monolayer-air interface remain very similar across all samples (inset, Fig. 3B), indicating that the protein primarily protrudes into the liquid phase, as schematized in Fig. 2A. Second, the integrated area under the step-like electron density profile revealed a net increase in total electrons per unit area (see shaded area in the inset of Fig. 3A), reinforcing the conclusion that ATP is synthase successfully incorporated into the monolayer. Remarkably, the increase in electron density was observed in the lipid polar-head region, suggesting a partial interpenetration of

the protein into the lipid monolayer. Similar results were obtained at lateral pressures $\pi = 30 \pm 2mN/m$ (see Fig. 3B and Fig. S2).

3.3. ATP synthase lowers the line tension of lipid domains

An additional proof for protein incorporation was obtained by assessing the line tension of lipid domains both in the presence and absence of ATP synthase [38]. Using high-speed video-microscopy, the contour fluctuations of bright or dark domains were recorded (Fig. 4A, inset). Contours of domains were then parameterized using a Fourier series to obtain the weight coefficients. Line tension, γ, was then calculated from the capillary wave spectrum, where the equipartition theorem distributes the thermal energy into different modes of fluctuation according to line tension of the interface. Values of line tension were obtained from the linear fit between the time-averaged of squared coefficients, $\langle a_n^2 \rangle + \langle b_n^2 \rangle$ of the fluctuation mode versus $1/(n^2-1)$ (Fig. 4A). We could first determine that line tension did not depend on the interfacial curvature, as the obtained values were similar for bright and dark domains ($\gamma_b = 1.0 \pm 0.5pN$ and $\gamma_d = 0.8 \pm 0.7pN$ for bright and dark domains, respectively) (Fig. 4B). Hereinafter, we will consider the overall value without considering whether the domain is bright or dark, $\gamma_{lipid} = 0.9 \pm 0.6pN (N = 21)$. This value is in agreement with data established by previous reports [39]. Interestingly, the incorporation of ATP synthase into the CL-rich phase reduced the line tension by one order of magnitude to $\gamma_{ATPsyn} = 0.09 \pm 0.08pN (N = 15)$ (Fig. 4B). The decrease of line tension reflects a change in lipid interactions within the CL-enriched phase by the incorporation of ATP synthase, in agreement with XRR data (Fig. 3). As previously shown in other systems [12], a decrease in line tension does not modify significantly the domain distribution.

3.4. Rotating ATP synthases modulate the size of domains

To determine the effect of protein activity to the dynamics and structural properties of lipid domains, ATP was added to the subphase (3.5 mM final concentration). After ATP injection, the size of lipid domains was noticeably modified after 1–15 min of incubation. Interestingly, CL-enriched bright domains increased their size whereas CL-voided dark domains became smaller (Fig. 5A). Remarkably, this effect was simultaneously observed in the same field of view on the same monolayer exhibiting similar fractions of bright or dark circular on a dark or bright background, respectively.

A first explanation for the observed change in the size of lipid domains might be sustained by a variation of the line tension, produced by the rotary motion of ATP synthases at the fluid–fluid interface. However, this mechanism would require a simultaneous increase and decrease in line tension in dark and bright domains, respectively. As the curvature of lipid domains is much lower than the size of proteins, a curvature-driven change in line tension is unlikely to occur. To further investigate this, we measured the line tension after the addition of ATP and compared it with the line tension in the absence of ATP, finding that it remained of the same order of magnitude; $\gamma_{ATPsyn}^{ATP} = 0.05 \pm 0.02pN (N = 14)$; or equivalently $\gamma_{ATPsyn}^{ATP}/\gamma_{ATPsyn} = 0.6 \pm 0.6$ (Fig. 4B).

An alternative mechanism for the size modulation of lipid domains by ATP synthase might be grounded on the elastic remodelling of lipid membranes by the spinning motion of the protein. Indeed, the rotation of the F_o domain of ATP synthase induces a decrease in the lateral pressure of lipid membranes [21]. Moreover, the relationship between size of lipid domains and difference in the lateral pressure across the interface is governed by the 2D version of the Young-Laplace equation:

$$\Delta\pi = \frac{\gamma}{R_0} \tag{1}$$

where $\Delta\pi$ is the surface pressure difference across the interface (higher inside; i.e. $\Delta\pi = \pi_i - \pi_o$), γ is the line tension of the interface and R_0 is the radius of the lipid domain. A change in $\Delta\pi$ by might lead to a variation in the size of domains. To compute the variation in the lateral pressure difference by the activity of ATP synthase we take the differential form of the Young-Laplace equation:

$$d(\Delta\pi) = \frac{d\gamma}{R_0} - \gamma\left(\frac{dR}{R_0^2}\right) \tag{2}$$

This equation implies that the change in the radius of domains is given by

$$-dR = \frac{d(\Delta\pi)}{\gamma}R_0^2 - \frac{d\gamma}{\gamma}R_0 \tag{3}$$

Fitting this equation to the experimental data (Fig. 5B) reveals that the change in radius is primarily driven by variations in lateral pressure

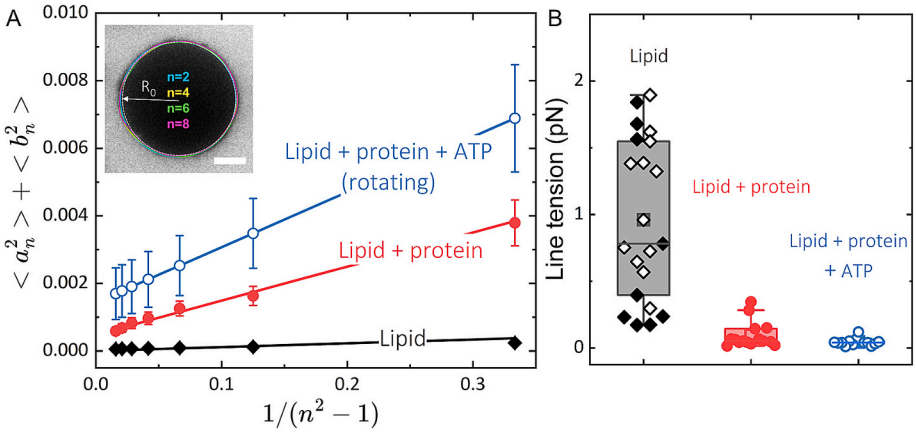

Fig. 4. A) Capillary wave spectra of domains in DPPC/Chol/DOPC/CL (50/30/10/10 % mol) monolayers in the absence (diamonds), presence of ATP synthase without (full circles) and with ATP (empty circles). Line tension, λ, is obtained from the linear fit of $\langle a_n^2 \rangle + \langle b_n^2 \rangle$ plotted vs. $1/(n^2-1)$ (see **Methods** for details). **Inset.** Fluorescence micrograph of a phase separated domain in a DPPC/Chol/DOPC/CL (50/30/10/10 % mol) monolayer. Fourier fluctuation analysis to obtain the capillary wave spectrum as calculated from the time-averaged variations in the domain radius compared to the mean radius, R_0 (scale bar is 5 μm). **B)** Box charts with the line tension values as obtained from the analyzed domains (N = 21, 15 and 14 for pure lipid monolayers (black and white diamonds represent dark and bright domains, respectively), monolayers with ATP synthase in the absence (full circles) and presence of ATP (empty circles), respectively from n = 3 independent samples). The box chart includes the mean value (square), the median (horizontal line), the confident interval between quartile Q1 and Q3 (box), and error bars as 1.5IQR, i.e. the interquartile range = Q3-Q1.

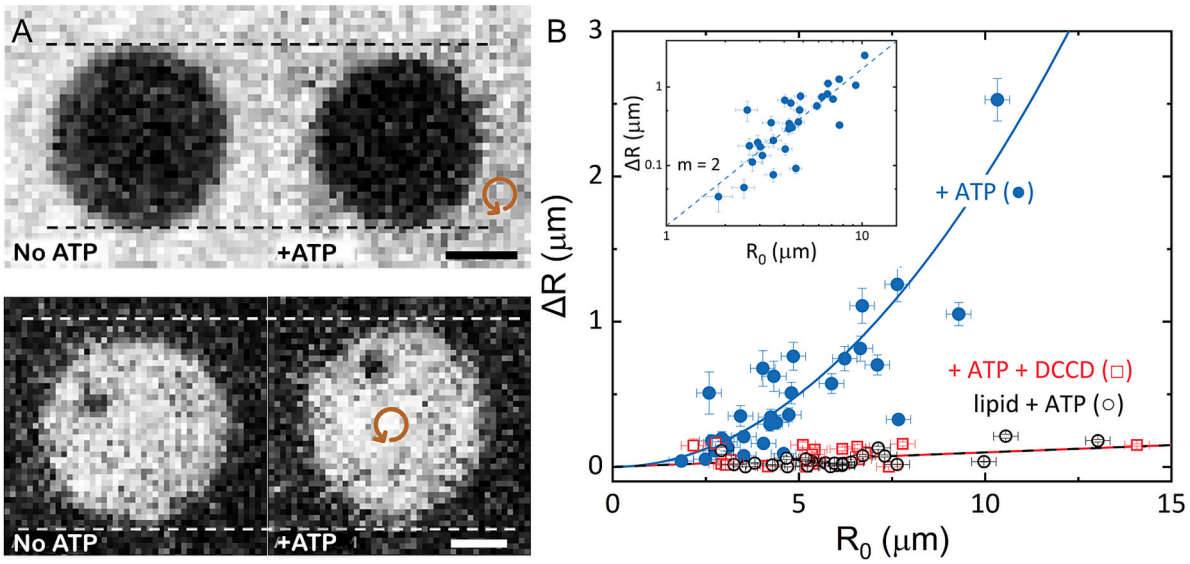

Fig. 5. **A)** Change in size of domains of DPPC/Chol/DOPC/CL (50/30/10/10 % mol) monolayers with a lipid-to-protein ratio of L/P = 10,000 at 20 mN/m and upon incubation with ATP. Bright phase is enriched in ATP synthase (see Fig. 2**B**). Whereas protein-enriched domains increase their size, protein-devoid domains became smaller in size. Circular arrows represent the direction of rotation by ATP synthases in bright phases. **B)** Variation in size of domains as a function of the initial radius. Dataset follows the Young-Laplace equation (fitting line corresponds to Eq.3). **Inset:** The quadratic scaling is better visualized in the log–log plot, with a slope of $m = 2.2 \pm 0.2$, as predicted by Eq. (4). Control experiments in the presence of the specific inhibitor DCCD, blocking the rotatory movement of ATP synthase (empty squares) or in the absence of ATP synthase (empty circles) did not exhibit a change in the size of domains upon incubation with ATP.

(first term), with negligible contribution from changes in line tension (second term) within the experimental range ($\frac{d(\Delta\pi)}{\gamma} = 0.018 \pm 0.004 \mu m^{-1}; \frac{d\gamma}{\gamma} = 0.006 \pm 0.03$). This observation is in agreement with the very similar line tension values observed in the presence or absence of ATP (Fig. 4B).

As expected, an increase in $\Delta\pi$ by the activity of proteins outside dark domains necessarily leads to $dR < 0$ and lipid domains decrease their size. Analogously, a decrease in $\Delta\pi$ by the activity of proteins inside bright domains results into $dR > 0$ and lipid domains increase their size. To explore the behavior in a more simplified manner, we linearize the equation with only the quadratic term in log–log scale.

$$log(dR) = 2logR_0 + log\left(\frac{d(\Delta\pi)}{\gamma}\right) \quad (4)$$

with the absolute values of dR and $d(\Delta\pi)$ for numerical reasons. This relationship helps to quantify the influence of ATP synthase's activity on the size of lipid domains in terms of the variation of the difference in lateral pressure across the interface and the line tension).

To check if the observed change in size of lipid domains upon protein rotation follows the Young-Laplace equation, leading to an active modulation of their size, the variation in radius, dR, was plotted as a function of the initial radius of domains, R_0, before ATP addition (Fig. 5B). The plot shows that dR scales quadratically with the initial radius of domains, as expected from Eq. (3). This scaling is clearer in the log–log plot of the inset, which shows a linear trend with slope of ($m = 2.2 \pm 0.2$), compatible with a slope of 2 as predicted by Eq. (4). Additionally, from the linear fit, we obtained $\frac{d(\Delta\pi)}{\gamma} = 0.018 \mu m^{-1}$ and calculated $d(\Delta\pi)$ using γ, as measured from the capillary wave spectrum (Fig. 4). Remarkably, unbalanced pressure differences as small as $d(\Delta\pi) \approx 10^{-9} N/m$; i.e. $\frac{d(\Delta\pi)}{\Delta\pi} \approx 10^{-3}$, are capable of changing the size of lipid domains.

An additional evaluation of the size modulation of lipid domains by rotational forces was experimentally addressed using N,N′-dicyclohexylcarbodiimide (DCCD, 1 mM final concentration) as a classical inhibitor of the ATP synthase. DCCD binds covalently to the spinning F_o domain of ATP synthase and thereby blocks its rotation [40]. Under the inhibitory conditions with the simultaneous incubation of DCCD and ATP, the size of lipid domains remained unchanged (Fig. 5B). Finally, we also evaluated the effect of incubating pure lipid monolayers with ATP and again, the size of lipid domains was unaltered (Fig. 5B). Thus, our results demonstrate a direct correlation between protein rotation and the change in size of lipid domains in phase-separated monolayers.

3.5. *Size modulation is driven by a decrease in the surface pressure of protein-enriched phase*

To reach these conclusions, we used simplified model systems in which membranes consisted of a single lipid monolayer, formed by spreading proteoliposomes onto the air–water interface. This approach offers the advantage of exhibiting extremely slow relaxation kinetics, where domain coalescence occurs over long timescales, keeping the domain distribution in a metastable state. Notably, during the experimental window, we did not observe significant domain fusion or fission. The observed effect of domain size modulation is therefore likely driven solely by the activity of the protein within the different CL-enriched phases.

CL is frequently seen as a proton trap, as this lipid has two phosphate-ester bonds with different pK that can be protonated at lower pH [41,42]. The emergence of change in the lateral pressure leading to the dynamic control of the size of lipid domains might be then triggered by the proton pump activity of ATP synthase close to the lipid interface. A localized pH drop near the CL-enriched phase would be the driving force for a change in the lipid packing [43,44]. However, lipid packing in cardiolipin CL-containing membranes increases at lower pH levels, as evidenced by a decrease in the zeta (ζ) potential and an increase in the generalized polarization (GP) of Laurdan [44]. Protonated CL reduces the long-ranged repulsion between lipid head-groups and as a result, lipids are able to pack more tightly within the membrane, leading to a denser and more ordered lipid arrangement. As the observed changes in domain size requires a drop in the lateral pressure of the CL-enriched phase (see Eq. (3)), protonation does not directly determine the observed phenomena but it might down-regulate the rotation-driven effect though. Alternatively, our observations show that domain size modulation aligns with the 2D Young-Laplace equation (Fig. 5),

confirming that protein rotation reduces the surface pressure of its embedded lipid phase [21], thereby driving the unbalanced surface pressure difference across the lipid phases.

3.6. Changes in domain size are not operated by mechanical deformation or Ostwald ripening

However, our experiments do not directly reveal the underlying process by which this surface pressure variation leads to domain growth and shrinkage. Either a mechanical or a transport-mediated process, among others, might operate the observed effect. In the mechanical case, domains would expand or contract without the incorporation of any additional lipids, i.e. undergoing stretching or compressing deformations, respectively. In the transport-mediated case, mass transfer in and out of the domains could drive their growth or shrinkage. Notably, the observed growth and reduction of domains following ATP synthase activation were restricted to domain sizes of 1 to $10\mu m$ in radius. Suitably, this limitation provides insight into the physical mechanism underlying domain size regulation.

Whereas the lower size limit is clearly determined by the optical resolution of the imaging system, the upper limit may be governed by the referred mechanical or diffusive constraints. One option is that mechanical stress, arising from the stretching/compression of domains, counterbalances the growth/shrinkage produced by the rotary movement of ATP synthase. However, this mechanical stress would likely only affect very small domains of $R \sim \frac{\gamma}{C_s^{-1}} \sim 10^{-9} m$ far below the micron-sized domains observed in our experiments.

Among various mass redistribution mechanisms, ripening typically transfers material from smaller domains to larger ones, resulting in an increase in the mean domain size and a decrease in the number of domains. This process is reversed for protein-devoid domains, where material would flow into smaller domains. However, we did not observe this typical behavior. Instead, the number of domains remained constant, further discarding ripening or merging effects. Alternatively, the increase/decrease in size after protein activation could involve a diffusive transport mechanism of lipids between different phases due to activation-induced affinity changes. The characteristic transport time for this process ,$t = R^2/D$, is estimated to range from 1 to 100 s for lipid diffusivity $D \sim 1\mu m^2/s$ and radius $R \sim 1-10\mu m$. For larger domains, these relaxation times may exceed the domain's lifetime before fusion with neighboring same-type domains. Furthermore, the proximity of complementary or competing same-type domains could limit the availability of lipids for domain growth/shrinkage. Additionally, the monolayer character of our experimental system may also play a critical role in the observed activation-induced size variations, as lipid monolayers present several anomalous hydrodynamic behaviours [45].

4. Conclusions

The size of lipid domains in phase-separated lipid monolayers is governed by a complex interplay of physicochemical parameters, including line tension, dipole–dipole interactions and kinetics phenomena [46]. Traditionally, domain size regulation has been linked to variations in line tension, which can be modulated by a number of factors, including applied surface pressure, thickness and lipid composition [47]. However, our study presents a novel approach to domain size regulation, wherein the surface pressure difference across the interface, rather than line tension alone, emerges as a key determinant of domain dynamics.

We propose that ATP synthase, through its rotary activity, drives changes in the surface pressure of its surrounding lipid phase [21], effectively creating an active, driven system capable of modulating lipid domain size in a controlled manner. To test this hypothesis, we used a simplified model membrane system in which ATP synthase was incorporated into cardiolipin (CL)-enriched monolayers exhibiting phase separation. Unlike bilayer-based systems, lipid monolayers offer the advantage of extremely slow kinetic relaxation [6,48], enabling us to observe domain dynamics over extended time scales while minimizing the effects of merging events. Our experiments confirmed that ATP synthase preferentially assembles into CL-enriched domains, reinforcing previous findings on its strong affinity for CL-rich environments [25,26].

Remarkably, we observed a dynamic modulation of lipid domain size upon ATP synthase activation, a phenomenon that could not be explained by passive equilibrium-based mechanisms alone but through the rotatory movement of the protein. The observed changes in domain size were consistent with a mechanism in which protein activity reduces the surface pressure of the rotor-enriched phase, resulting in an unbalanced pressure difference across the lipid phases. This imbalance drives domain expansion and shrinkage in accordance with the 2D Young-Laplace equation, providing a mechanistic link between protein function and membrane mechanics.

To further examine the operating mechanism, we ruled out classical processes such as Ostwald ripening, domain coalescence and purely mechanical deformations; all of which would have led to different time scale behaviors or operate only on very small domains. Instead, our data suggest a diffusion-mediated process, constrained by the physical properties of the monolayer, where lipid redistribution occurs between coexisting phases likely due to activation-induced changes in molecular packing and affinity.

Overall, our findings establish ATP synthase as an active driver of membrane remodeling, demonstrating a functional connection between nanoscale protein activity and large-scale membrane organization. These results not only provide new insights into how biological membranes achieve dynamic control over domain organization [46] but also open new avenues for engineering functional nanomaterials. Future studies will be crucial in determining whether other membrane proteins exert similar effects and how such active remodeling mechanisms contribute to cellular membrane homeostasis.

CRediT authorship contribution statement

Nuria Carrillo-Godoy: Writing – review & editing, Investigation, Data curation. **David Valdivieso González:** Writing – review & editing, Investigation. **Paolo Natale:** Writing – review & editing, Resources, Methodology. **Hernán Ritacco:** Writing – review & editing, Writing – original draft, Investigation, Data curation. **Francisco J. Cao-García:** Writing – original draft, Formal analysis. **Víctor G. Almendro-Vedia:** Writing – review & editing, Supervision, Data curation. **Iván López-Montero:** Writing – review & editing, Writing – original draft, Supervision, Funding acquisition, Conceptualization.

Declaration of competing interest

The authors declare that they have no known competing financial interests or personal relationships that could have appeared to influence the work reported in this paper.

Acknowledgements

I.L.-M. acknowledges financial support from the Spanish Ministry of Science, Innovation and Universities through the grant PID2021-125024NB-C22. N.C.-G. also acknowledges the Spanish Ministry of Science, Innovation and Universities for the PhD grant (PRE2022-101514). D.V.G. acknowledges University Complutense of Madrid and Banco Santander for PhD Grant (CT58/21-CT59/21). F.J.C.-G. was supported by the Spanish Ministry of Science, Innovation and Universities through the grant PID2023-148319NB-I00; and by Universidad Complutense de Madrid (UCM) through the grant PR12/24-31558. H.R. thanks Agencia Nacional de Promoción Científica y Tecnológica (ANPCyT), Argentina (grant PICT-2019-3185), Consejo Nacional de Investigaciones Científicas y Técnicas (CONICET), Argentina (grant PIP

11220200101754CO) and the Universidad Nacional del Sur (UNS), Argentina (grant PGI-UNS 24/F091) for financial support. Authors thank Dr. Marcos Fernández Leyes for helping with XRR measurements and setup.

Appendix A. Supplementary data

Supplementary data to this article can be found online at https://doi.org/10.1016/j.jcis.2025.138061.

Data availability

Data will be made available on request.

References

[1] F.A. Heberle, G.W. Feigenson, Phase Separation in lipid membranes, Cold Spring Harb. Perspect. Biol. 3 (2011) a004630–a, https://doi.org/10.1101/cshperspect.a004630.
[2] V.A.J. Frolov, Y.A. Chizmadzhev, F.S. Cohen, J. Zimmerberg, "Entropic traps" in the kinetics of phase Separation in multicomponent membranes stabilize nanodomains, Biophys. J . 91 (2006) 189–205, https://doi.org/10.1529/biophysj.105.068502.
[3] F. Vega Mercado, B. Maggio, N. Wilke, Modulation of the domain topography of biphasic monolayers of stearic acid and dimyristoyl phosphatidylcholine, Chemistry and Physics of Lipids 165 (2012) 232–237, https://doi.org/10.1016/j.chemphyslip.2012.01.003.
[4] C.D. Blanchette, W.-C. Lin, C.A. Orme, T.V. Ratto, M.L. Longo, Using nucleation rates to determine the Interfacial line tension of symmetric and Asymmetric lipid bilayer domains, Langmuir 23 (2007) 5875–5877, https://doi.org/10.1021/la7004584.
[5] T. Baumgart, S. Das, W.W. Webb, J.T. Jenkins, Membrane elasticity in Giant vesicles with fluid phase coexistence, Biophys. J . 89 (2005) 1067–1080, https://doi.org/10.1529/biophysj.104.049692.
[6] S.L. Keller, H.M. McConnell, Stripe phases in lipid monolayers near a miscibility critical point, PhysRevLett.8 82 (1999) 1602–1605, https://doi.org/10.1103/PhysRevLett.82.1602.
[7] Y. Hu, K.Y.C. Lee, J. Israelachvili, Sealed minitrough for microscopy and long-term stability studies of langmuir monolayers, Langmuir 19 (2003) 100–104, https://doi.org/10.1021/la026372y.
[8] A.J. García-Sáez, S. Chiantia, P. Schwille, Effect of line tension on the lateral Organization of Lipid Membranes, J. Biol. Chem. 282 (2007) 33537–33544, https://doi.org/10.1074/jbc.M706162200.
[9] F.A. Heberle, R.S. Petruzielo, J. Pan, P. Drazba, N. Kučerka, R.F. Standaert, G. W. Feigenson, J. Katsaras, Bilayer thickness mismatch controls domain size in model membranes, J. Am. Chem. Soc. 135 (2013) 6853–6859, https://doi.org/10.1021/ja3113615.
[10] B. Palmieri, T. Yamamoto, R.C. Brewster, S.A. Safran, Line active molecules promote inhomogeneous structures in membranes: theory, simulations and experiments, Adv. Colloid Interface Sci. 208 (2014) 58–65, https://doi.org/10.1016/j.cis.2014.02.007.
[11] L. Scheidegger, L. Stricker, P.J. Beltramo, J. Vermant, Domain size regulation in phospholipid model membranes using oil molecules and hybrid lipids, J. Phys. Chem. B 126 (2022) 5842–5854, https://doi.org/10.1021/acs.jpcb.2c02862.
[12] A.A. Bischof, A. Mangiarotti, N. Wilke, Searching for line active molecules on biphasic lipid monolayers, Soft Matter 11 (2015) 2147–2156, https://doi.org/10.1039/C5SM00022J.
[13] P.D. Boyer, The atp synthase—a splendid molecular machine, Annu. Rev. Biochem. 66 (1997) 717–749, https://doi.org/10.1146/annurev.biochem.66.1.717.
[14] P. Mitchell, Chemiosmotic coupling in oxidative and photosynthetic phosphorylation, Biol. Rev. 41 (1966) 445–501, https://doi.org/10.1111/j.1469-185X.1966.tb01501.x.
[15] Y. Sambongi, Y. Iko, M. Tanabe, H. Omote, A. Iwamoto-Kihara, I. Ueda, T. Yanagida, Y. Wada, M. Futai, Mechanical rotation of the c subunit Oligomer in ATP synthase (F_0F_1): direct observation, Science 286 (1999) 1722–1724, https://doi.org/10.1126/science.286.5445.1722.
[16] B.A. Grzybowski, H.A. Stone, G.M. Whitesides, Dynamic self-assembly of magnetized, millimetre-sized objects rotating at a liquid–air interface, Nature 405 (2000) 1033–1036, https://doi.org/10.1038/35016528.
[17] B.A. Grzybowski, G.M. Whitesides, Dynamic aggregation of chiral spinners, Science 296 (2002) 718–721, https://doi.org/10.1126/science.1068130.
[18] B.C. Van Zuiden, J. Paulose, W.T.M. Irvine, D. Bartolo, V. Vitelli, Spatiotemporal order and emergent edge currents in active spinner materials, Proc. Natl. Acad. Sci. U.S.A. 113 (2016) 12919–12924, https://doi.org/10.1073/pnas.1609572113.
[19] P. Lenz, J.-F. Joanny, F. Jülicher, J. Prost, Membranes with rotating motors, Phys. Rev. Lett. 91 (2003) 108104, https://doi.org/10.1103/PhysRevLett.91.108104.
[20] N. Oppenheimer, D.B. Stein, M.J. Shelley, Rotating membrane inclusions crystallize through hydrodynamic and steric Interactions, Phys. Rev. Lett. 123 (2019) 148101, https://doi.org/10.1103/PhysRevLett.123.148101.
[21] D. Valdivieso González, M.A. Sacristán, P. Natale, B. Orgaz, M.P. Lillo, V. G. Almendro-Vedia, I. Lopez-Montero, Elastic remodelling of model and cell membranes by rotating ATP synthase, Cell Rep. Phys. Sci. 6 (2025) 102567, https://doi.org/10.1016/j.xcrp.2025.102567.
[22] V.G. Almendro-Vedia, P. Natale, M. Mell, S. Bonneau, F. Monroy, F. Joubert, I. López-Montero, Nonequilibrium fluctuations of lipid membranes by the rotating motor protein F_1 F_0 -ATP synthase, Proc. Natl. Acad. Sci. U.S.A. 114 (2017) 11291–11296, https://doi.org/10.1073/pnas.1701207114.
[23] D. Valdivieso González, M. Makowski, M.P. Lillo, F.J. Cao-García, M.N. Melo, V. G. Almendro-Vedia, I. López-Montero, Rotation of the *c*-ring promotes the curvature sorting of Monomeric ATP synthases, Adv. Sci. 10 (2023) 2301606, https://doi.org/10.1002/advs.202301606.
[24] B.L. Stottrup, D.S. Stevens, S.L. Keller, Miscibility of Ternary mixtures of phospholipids and cholesterol in monolayers, and application to bilayer systems, Biophys. J. 88 (2005) 269–276, https://doi.org/10.1529/biophysj.104.048439.
[25] M. Sobti, J.L. Walshe, D. Wu, R. Ishmukhametov, Y.C. Zeng, C.V. Robinson, R. M. Berry, A.G. Stewart, Cryo-EM structures provide insight into how E. coli F1Fo ATP synthase accommodates symmetry mismatch, Nat. Commun. 11 (2020) 2615, https://doi.org/10.1038/s41467-020-16387-2.
[26] R.A. Corey, W. Song, A.L. Duncan, T.B. Ansell, M.S.P. Sansom, P.J. Stansfeld, Identification and assessment of cardiolipin interactions with *E. coli* inner membrane proteins, Sci. Adv. 7 (2021) eabh2217, https://doi.org/10.1126/sciadv.abh2217.
[27] Ó. Gutiérrez-Sanz, P. Natale, I. Márquez, M.C. Marques, S. Zacarias, M. Pita, I.A. C. Pereira, I. López-Montero, A.L. De Lacey, M. Vélez, H_2 -fueled ATP synthesis on an electrode: mimicking Cellular respiration, Angew. Chem. Int. Ed. 55 (2016) 6216–6220, https://doi.org/10.1002/anie.201600752.
[28] H. Martinelli, C. Domínguez, M.F. Leyes, S. Moya, H. Ritacco, A pH-responsive foam formulated with PAA/Gemini 12-2-12 complexes, Colloids and Interfaces 5 (2021) 37, https://doi.org/10.3390/colloids5030037.
[29] L.G. Parratt, Surface studies of solids by Total reflection of X-rays, PhysRev.9 95 (1954) 359–369, https://doi.org/10.1103/PhysRev.95.359.
[30] S. Morein, A.-S. Andersson, L. Rilfors, G. Lindblom, Wild-type Escherichia coli cells regulate the membrane lipid composition in a "window" between gel and non-lamellar structures, J. Biol. Chem. 271 (1996) 6801–6809, https://doi.org/10.1074/jbc.271.12.6801.
[31] O. Schiaffarino, D. Valdivieso González, I.M. García-Pérez, D.A. Peñalva, V. G. Almendro-Vedia, P. Natale, I. López-Montero, Mitochondrial membrane models built from native lipid extracts: Interfacial and transport properties, Front. Mol. Biosci. 9 (2022) 910936, https://doi.org/10.3389/fmolb.2022.910936.
[32] S. Nichols-Smith, S.-Y. Teh, T.L. Kuhl, Thermodynamic and mechanical properties of model mitochondrial membranes, Biochim. Biophys. Acta Biomembr. 1663 (2004) 82–88, https://doi.org/10.1016/j.bbamem.2004.02.002.
[33] Ò. Domènech, F. Sanz, M.T. Montero, J. Hernández-Borrell, Thermodynamic and structural study of the main phospholipid components comprising the mitochondrial inner membrane, Biochim. Biophys. Acta Biomembr. 1758 (2006) 213–221, https://doi.org/10.1016/j.bbamem.2006.02.008.
[34] J.D. Unsay, K. Cosentino, Y. Subburaj, A.J. García-Sáez, Cardiolipin effects on membrane structure and dynamics, Langmuir 29 (2013) 15878–15887, https://doi.org/10.1021/la402669z.
[35] M.D. Phan, K. Shin, Effects of Cardiolipin on membrane morphology: a langmuir monolayer study, Biophys. J . 108 (2015) 1977–1986, https://doi.org/10.1016/j.bpj.2015.03.026.
[36] S.M. Danauskas, D. Li, M. Meron, B. Lin, K.Y.C. Lee, Stochastic fitting of specular X-ray reflectivity data using *StochFit*, J Appl Crystallogr 41 (2008) 1187–1193, https://doi.org/10.1107/S0021889808032445.
[37] C.A. Helm, H. Möhwald, K. Kjær, J. Als-Nielsen, Phospholipid monolayer density distribution Perpendicular to the water Surface. a synchrotron X-ray reflectivity study, Europhys. Lett. 4 (1987) 697–703, https://doi.org/10.1209/0295-5075/4/6/010.
[38] B.L. Stottrup, A.M. Heussler, T.A. Bibelnieks, Determination of line tension in lipid monolayers by fourier analysis of Capillary waves, J. Phys. Chem. B 111 (2007) 11091–11094, https://doi.org/10.1021/jp074898r.
[39] B.L. Stottrup, J. TigreLazo, V.B. Bagonza, J.C. Kunz, J.A. Zasadzinski, Comparison of line tension measurement methods for lipid monolayers at liquid–liquid coexistence, Langmuir 35 (2019) 16053–16061, https://doi.org/10.1021/acs.langmuir.9b01696.
[40] J. Hermolin, R.H. Fillingame, H+-ATPase activity of Escherichia coli F1F0 is blocked after reaction of dicyclohexylcarbodiimide with a single proteolipid (subunit c) of the F0 complex, J. Biol. Chem. 264 (1989) 3896–3903, https://doi.org/10.1016/S0021-9258(19)84937-2.
[41] G. Olofsson, E. Sparr, Ionization constants pKa of Cardiolipin, PLoS One 8 (2013) e73040, https://doi.org/10.1371/journal.pone.0073040.
[42] M. Sathappa, N.N. Alder, The ionization properties of cardiolipin and its variants in model bilayers, Biochim. Biophys. Acta Biomembr. (1858 (2016)) 1362–1372, https://doi.org/10.1016/j.bbamem.2016.03.007.
[43] N. Khalifat, N. Puff, S. Bonneau, J.-B. Fournier, M.I. Angelova, Membrane deformation under local pH gradient: mimicking mitochondrial cristae dynamics, Biophys. J . 95 (2008) 4924–4933, https://doi.org/10.1529/biophysj.108.136077.
[44] N. Khalifat, J.-B. Fournier, M.I. Angelova, N. Puff, Lipid packing variations induced by pH in cardiolipin-containing bilayers: the driving force for the cristae-like shape instability, Biochim. Biophys. Acta Biomembr. 1808 (2011) 2724–2733, https://doi.org/10.1016/j.bbamem.2011.07.013.
[45] T.J. Mucci, B.L. Liu, J.A. Adam, A.H. Hirsa, J. Yalim, J.M. Lopez, Nonequilibrium interfacial diffusivity resolves anomalies in monolayer hydrodynamics, PhysRevE 111 (2025) L013501, https://doi.org/10.1103/PhysRevE.111.L013501.
[46] C.M. Rosetti, A. Mangiarotti, N. Wilke, Sizes of lipid domains: what do we know from artificial lipid membranes? what are the possible shared features with

membrane rafts in cells? Biochim. Biophys. Acta Biomembr. 1859 (2017) 789–802, https://doi.org/10.1016/j.bbamem.2017.01.030.

[47] I. Sriram, D.K. Schwartz, Line tension between coexisting phases in monolayers and bilayers of amphiphilic molecules, Surf. Sci. Rep. 67 (2012) 143–159, https://doi.org/10.1016/j.surfrep.2012.02.002.

[48] H.M. McConnell, Structures and transitions in lipid monolayers at the air-water Interface, Annu. Rev. Phys. Chem. 42 (1991) 171–195, https://doi.org/10.1146/annurev.pc.42.100191.001131.